Microglia-derived FGF21 as a modulator of astrocytic phenotype and cerebral ischemia injury

Fei Liu
Wenzhou Medical University
Dongxue Wang
Wenzhou Medical University
Liyun Zhu
Wenzhou Medical University
Jingting Du
Wenzhou Medical University
Ping Lin
Wenzhou Medical University
Fei Liang
Wenzhou Medical University
Xue Wang
Wenzhou Medical University
Xianxi Tan
Wenzhou Medical University First Affiliated Hospital
Li Lin (linliwz@163.com)
Wenzhou Medical University

Research

Keywords: FGF21, MCAO/reperfusion, microglia, astrocytes, phenotype

Posted Date: March 3rd, 2020

DOI: https://doi.org/10.21203/rs.3.rs-15781/v1

Abstract

Background: Fibroblast growth factor 21 (FGF21) is an important neuroprotective factor in the central nervous system (CNS), and it has been reported that FGF21 can protect against cerebral ischemia during the acute phase. However, the possible effects of FGF21 on ischemic brains and the interactions between FGF21 and nonneuronal cells have not been examined. Thus, the aim of this study was to elucidate the protective effects of endogenous FGF21 in ischemic brains.

Methods: In this study, in vivo ischemia/reperfusion injury mouse model established by transient middle cerebral artery occlusion (MCAO)/reperfusion and in vitro cell models of oxygen/glucose deprivation (OGD)/reoxygenation (R) were used. Western blot analysis, RT-PCR, double immunofluorescence staining, immunohistochemistry, 2,3,5-triphenyltetrazolium chloride (TTC) staining, hematoxylin-eosin (H&E) staining, neurobehavioral tests, cell counting kit-8 (CCK-8) assay and high-throughput gene sequencing were employed to explore the mechanism by which FGF21 unleash neuroprotective effort of astrocyte phenotype shifts in ischemic stroke.

Results: We found that cortical FGF21 expression significantly increased after MCAO/reperfusion, peaking at 7 d. Ischemia-activated microglia were the main sources of endogenous FGF21 in brain tissue. However, FGF21 deficiency aggravated brain injury and slowed neurological functional recovery in FGF21 knockout mice. The in vitro and vivo studies revealed that FGF21 could activate astrocytes and mediate astrocytic phenotype. FGF21-activated astrocytes contributed to neuronal survival and synaptic protein upregulation after ischemia.

Conclusion: Collectively, our data indicate that FGF21 plays vital roles in alleviating ischemic brain by mediating the manifestation of potentially pro-recovery astrocytic phenotypes. Therefore, modulation of FGF21 is a potential target strategy for stroke.

Background

Ischemic stroke is a common neurological injury and the third leading cause of disability and death in China [1]. Unfortunately, the physiopathological mechanism of ischemic stroke is complex, and recombinant tissue-type plasminogen activator (rt-PA) is considered to be the most effective treatment agent [2, 3]. However, intravenous thrombolysis fails to show excellent therapeutic effects against ischemic stroke. After cerebral blood flow is restored, the postischemic inflammatory response and several detrimental factors, including excitotoxic neurotransmitters and cytokines, cause further neuronal injury [1]. Elucidation of the mechanisms of neuronal injury and repair in order to reduce the severity of neurological diseases and discovery of other efficacious treatments targeting neuronal protection are urgently needed.

Currently, endogenous neuronal protection is a promising strategy for neurological recovery and regeneration after ischemic injury [4]. The effects and functions of nonneuronal cells, such as microglia and astrocytes, supporting neuronal survival should not be neglected [5]. Accumulating evidence

suggests that circulating factors released by glia subjected to ischemia play important roles in the pathogenesis of stroke [6]. Microglia, the brain-resident phagocytes, can be activated in response to brain injury and diseases and are involved in neuroinflammation in ischemic brains [7, 8]. Microglia, especially those of the M2 phenotype, can promote brain repair by producing trophic factors, which are potentially helpful for neurons and can remove apoptotic neurons to balance the microenvironment in ischemic brains [9]. For instance, interleukin-10 (IL-10) from M2 microglia attenuates local inflammatory reactions by downregulating the expression of proinflammatory cytokines and chemokines after ischemic stroke [10]. In addition, Ma et al. further demonstrated that microglia exert a protective role by releasing neurotrophic factors, such as brain-derived neurotropic factor (BDNF), insulin-like growth factor 1 (IGF-1), and nicotinamide phosphoribosyl transferase (NAMPT) [11, 12]. Similarly, astrocytes, the most abundant glial cells in the central nervous system (CNS), can be induced to develop different phenotypes depending on the damage and the phase [13]. In contrast to A1 astrocytes, which upregulate classic complement cascade genes and are destructive to synapses, A2 astrocytes participate in the regulation of neurodevelopment and the promotion of synapse formation by producing neurotrophic factors [14]. Previous studies have shown that growth and nutritional factors or proteins (DJ-1, MEGF10), which can sustain astrocytic neuroprotection, are synthesized and secreted by A2 astrocytes [15]. Recently, DJ-1 has been found to induce neuroprotection by mediating the Nrf2/ARE pathway [16]. In addition, Chung et al. have reported that astrocytes actively contribute to synapse elimination in the developing CNS via astrocytic MEGF10 [17]. Furthermore, other endogenous trophic factors, such as FGF10 and FGF2, produced by ischemic brains are essential for brain repair, as they inhibit NF-κB-dependent neuroinflammation and upregulate the expression of PDGFRβ [18, 19]. However, more work is needed to elucidate the roles of other factors from glia in ischemic brains.

FGF21 is a unique member of the FGF superfamily [20], and its role in type 2 diabetes related to the promotion of insulin synthesis and secretion has been studied widely [21]. It has also been revealed that exogenous FGF21 administration ameliorates ischemia-reperfusion injury in cardiomyocytes [22], improving the antioxidant capacity of endothelial cells [23]. Moreover, a growing body of evidence supports the notion that FGF21 can be released by brain tissue [24]. Under pathological conditions, FGF21 acts as a therapeutic factor, improving insulin sensitivity and glucose uptake to attenuate metabolic stress-induced Alzheimer disease pathology [25]. Chen et al demonstrated that FGF21 protects the blood-brain barrier by forming an FGF21/FGFR1/β-klotho complex and activating PPAR-γ after traumatic brain injury [26]. However, animal model studies on neurological diseases have paid no attention to the effects and detailed mechanisms of endogenous FGF21, and the potential efficacy of endogenous FGF21 under physiological conditions is not clear.

Hence, we hypothesized that endogenous FGF21 is an urgent neuroprotective modulator serving to ameliorate brain damage induced by ischemia/reperfusion. The aim of the present study was to examine the functions of endogenous FGF21 during long-term brain rehabilitation after ischemic stroke and to explore more neuroprotective mechanisms between FGF21 and nonneuronal cells.

Materials And Methods

Animals models

All animal experiments were authorized by the Laboratory Animal Ethics Committee of Wenzhou Medical University, and the procedures were conducted in compliance with the National Institutes of Health Guide for the Care and Use of Laboratory Animals. Wild-type male C57BL/6 mice weighing 20-25 g were obtained from the Animal Center of the Chinese Academy of Sciences (Shanghai, China), and FGF21 knockout (KO) male C57BL/6 mice were supplied by Chinese-American Research Institute for Diabetic Complications (Wenzhou Medical University, China).

These mice were subjected to transient middle cerebral artery occlusion (MCAO)/reperfusion as previously described [27]. In brief, each animal was anesthetized with isoflurane, and its rectal temperature was maintained at 36.5 ℃-37.5 ℃. The right common carotid artery (CCA) was isolated, and the internal carotid artery (ICA) and external carotid artery (ECA) were exposed. Then, a silicone rubber-coated nylon monofilament was inserted into the right middle cerebral artery (MCA). A laser Doppler flowmeter (MedWrench, Brentwood, USA) was used to detect cerebral blood flow (CBF), and mice with CBF reductions of more than 80% compared with the baseline were selected. The occluding filament was withdrawn after 80 min to allow reperfusion.

Recombinant human FGF21 (rhFGF21) (Wenzhou Medical University, China) was dissolved in a sterile 0.9% normal saline solution. rhFGF21 (1.5 mg/kg) or vehicle control (sterile 0.9% normal saline solution, the volume of vehicle is the same as that of rhFGF21 solution) were injected intraperitoneally at the end of reperfusion, and were administered at 24 h intervals for 7 d.

Immunohistochemistry and image analysis

On 7 d, brains were removed and post-fixed in 4% PFA at 4 °C overnight. Subsequently, the brains were embedded in paraffin and sectioned into 5 μm slices. Followed by xylene deparaffination, ethanol rehydration, and incubated with 3% H_2O_2 (diluted in PBS solution) for 15 min. Then, the sections were boiled in citrate buffer for 2 min to retrieve antigen, and nonspecific antibody binding was blocked by 5% bovine serum albumin (BSA) for 30 min at 37 °C. Rabbit monoclonal anti-FGF21 (1:250, ab171941, Abcam) were incubated with tissue sections at 4 °C overnight, followed by incubation in goat anti-rabbit secondary antibody (1:800, ab6721, Abcam) for 2 h at 37 °C. Sections were colored with DAB-kit (ZSGB-BIO, Beijing, China), and then counter stained with hematoxylin (Beyotime Institute of Biotechnology, Shanghai, China). Finally, the resulting images were examined under white light using a Nikon ECLIPSE 80i microscope (Nikon, Tokyo, Japan) and analyzed using ImageJ software. The percent of ipsilateral FGF21-positive area increase was calculated using the following formula: [1-(area of ipsilateral FGF21 staining/area of contralateral FGF21 staining)] ×100%.

Double immunofluorescence staining

As we formerly described [26], sections were blocked with 5% BSA for 1 h at 37 °C, and incubated with mouse monoclonal anti-FGF21 (1:300, NBP2-67275, NOVUS), along with different markers including Rabbit monoclonal anti-NeuN (1:300, ab177487, Abcam), Goat polyclonal anti-GFAP (1:400, ab53554, Abcam), and Goat polyclonal anti-Iba1 (1:500, ab48004, Abcam) at 4 °C overnight. Then the sections were treated with Alexa Flour 488-conjugated donkey anti-mouse IgG (1:800, ab150105, Abcam), Alexa Flour 647-conjugated donkey anti-goat IgG (1:200, ab150131, Abcam) or Alexa Flour 647-conjugated donkey anti-rabbit IgG (1:1000, ab150075, Abcam) for 1 h at 37 °C. After rinsed by PBST, Fluoroshield Mounting Medium with DAPI (ab104139, Abcam) was used to stain the cell nuclei. All fluorescence images were observed using a Leica confocal laser microscope (Leica, Wetzlar, Germany).

Neurobehavioral tests

mNSS scores

To evaluate neurological deficits, modified neurological severity scores (mNSSs) were performed over 14 d after MCAO/reperfusion as reported previously [28]. Briefly, mNSSs were graded on a scale of 0-18, mice were assessed for motor, reflex and sensory performance. The scores were awarded when mice were unable to perform the tests or lacked the tested reflexes as mentioned. The higher the scores represented strict damage.

Corner turning test

The corner test was used to access sensorimotor abnormalities as previous described [29]. A corner was made with an angle of 30° using two cardboard pieces, and then mice entered the corner spontaneously. Normal mice turned either left or right, while MCAO/reperfusion induced-mice preferentially turned toward the left (ischemic) side. The percentage of left over 20 trials were calculated.

Forelimb grip strength

Forelimb grip strength of mice was tested by a recording grip meter according to reported [30]. In brief, mice were held by tail and allowed to grasp a wire ring in diameter connected to a strain gauge. The force required to pull the subject away from the wire was recorded as the measure of the grip strength.

Rotarod test

To judge motor balance and coordination, the rotarod test was performed using a rotarod apparatus (Comerio, Solbiate Olona, Italy) on the basis of JK *et al* [31]. After placed onto the rungs of the accelerating rotarod, in which the speed increased slowly from 5 to 40 rpm over 4 min, the time that mice remained on the rotarod was measured. The mean duration (in seconds) over three individual trials was recorded.

Infract volume measurement

3 d after MCAO/reperfusion, the brains were quickly removed and sliced into 2-mm-thick sections. The brain slices were immersed in cold 1% 2,3,5-triphenyltetrazolium chloride (TTC, Sigma-Aldrich, Missouri, USA) for 15 min at 37 °C in dark, and then fixed in 4% paraformaldehyde at 4 °C overnight. The infarct area in white of each section was measured by Image J software. Percentage of infarct volume was calculated using the following equation: [(contralateral hemisphere volume-uninfracted area of ipsilateral hemisphere volume)/contralateral hemisphere volume×2] ×100%

Histological staining

Hematoxylin-eosin (H&E) staining was performed to evaluate the histopathological changes of brains based on the previous protocol [32]. Brain sections were dried at 60-65 ℃ for 30 min, brain sections were subjected to H&E solution (Beyotime Institute of Biotechnology) after deparaffinized and rehydrated. Images were captured using a Nikon Eclipse 80i microscope (Nikon) and analyzed by ImageJ software. The residual volume was calculated using the following formula: (ipsilateral hemisphere volume /contralateral hemisphere volume) ×100%.

Primary cortical neuron cultures

Primary cortical neurons were prepared from embryonal brains (16–18 d) of Sprague–Dawley rats as we previously described [33]. Briefly, the separated cortices were digested by 0.25% trypsin-EDTA (Invitrogen, California, USA), and were filtered by cell strainer. Then the dissociated cortical cells were seeded at poly-D-lysine (Sigma-Aldrich) coated culture plates, and cultured in DMEM containing 5% FBS and 1% Pen/Strep at a density of 3×10^5 cell ml^{-1} (3 ml for 6-well cell culture plate, 0.5 ml for 24-well cell culture plate). After 20 h of seeding, neurobasal medium (Invitrogen) containing 2% B27 (Invitrogen), 0.5 mM L-glutamine (Sigma-Aldrich) and 1% Pen/Strep replaced the medium. The neurons cultured 8-9 days after seeding were used for further analysis.

Primary microglia and astrocyte cultures

Cortical microglia and astrocyte cultures were isolated and purified from 2-day-old neonatal Sprague–Dawley rats as reported previously [34]. In brief, after digesting and filtering, the mixed cells were plated on 75 cm^2 flasks and cultured in DMEM/F12 medium containing 10% FBS and 1% Pen/Strep for 14 d. Mixed medium with a trypsin solution (0.25% trypsin diluted 1:4 in DMEM/F12) were induced for 30 min, microglia still remained attached to the bottom of the well, while other cells were detached [35].

Mixed glial cultures were shake at 220 rpm for 4 h, and at 180 rpm overnight to remove non-astrocytic cells. Astrocytes were dissected and reseeded on poly-L-lysine-coated plates. After the cells reached 80–90% confluence, cultures were treated with vehicle- or 100 nM of recombinant human FGF21 (rhFGF21) (Wenzhou Medical University, China) for 4 h, and cultures were switched to neurobasal medium containing 2% B27, 0.5 mM L-glutamine and 1% Pen/Strep subsequently. Another 24 h later, astrocytic conditioned medium was collected, and were transferred to neurons during the reoxygenation for further experiments.

Oxygen glucose deprivation (OGD)/Reoxygenation (R)

For OGD/R treatment, the cell cultures were subjected as previously reported [36]. After 30 min of OGD, the primary cultures (neurons, microglia and astrocyte) were replaced with normal medium, and cells were allowed to reoxygenation for 24 h for protein expression assay. On the other hand, neuron cultures were transferred to an anaerobic chamber for 2 h. At the end of OGD treatment, conditioned medium from astrocytes were added, and the cultures were placed in normal atmosphere for 24 h.

Western blotting analysis

The brain tissues and cells were homogenized in RIPA lysis buffer (Sigma-Aldrich), 1% PMSF (Beyotime Institute of Biotechnology) and 1% phosphatase inhibitors (Solarbio, Beijing, China). BCA protein assay kit was used to measure the protein concentrations, and amount of protein (100 μg *in vivo* and 50 μg *in vitro*) were applied. Then, the membranes were followed by blocking with 5% nonfat milk for 2 h at room temperature, and incubated with primary antibodies at 4 °C overnight. The primary antibodies used including rabbit monoclonal anti-FGF21 (1:1000, ab171941, Abcam), goat polyclonal anti-TGF-β (1:1000, ab92486, Abcam), rabbit polyclonal anti-PSD95 (1:1000, ab18258, Abcam), rabbit monoclonal anti-synaptophysin (1:20000, ab32127, Abcam), rabbit polyclonal anti-synaptotagmin1 (1:1000, ab131551, Abcam), rabbit monoclonal anti-BDNF (1:1000, BS9896M, Bioworld), mouse monoclonal anti-Thbs-1 (1 μg/ml, MS-418-PABX, Thermo fisher), mouse monoclonal anti-VEGF (1:500, sc-7269, Santa Cruz), mouse monoclonal anti-IGF-1 (1:500, sc-518040, Santa Cruz), mouse monoclonal anti-MAP2 (1:800, sc-74421, Santa Cruz), rabbit polyclonal anti-β-Actin (1:3000, AP0060, Bioworld), and rabbit monoclonal anti-GAPDH (1:3000, 5174, CST). The second day, membranes were incubated with the appropriate secondary antibodies (goat anti-mouse, 1:10,000, BS12478, Bioworld; goat anti-rabbit, 1:30,000, ab6721, Abcam) for 1 h at room temperature. The bands were visualized with an ECL kit, and then were detected using a ChemiDoc XRS+ Imaging System (Bio-Rad, California, USA). The gray values of the bands were analyzed using Image Lab 6.0 software (Bio-Rad).

Cell counting kit-8 (CCK-8) assay

Cellular viability was subjected to CCK-8 (Beyotime Institute of Biotechnology) assay. After cells were treated, the CCK-8 solution was added to the culture medium (CCK-8 diluted 1:10 in medium), which were then incubated in the dark for 4 h at 37 °C. The optical density (OD) was measured at 450 nm (BioTek, Winooski, VT, USA). The percentage of cellular viability was calculated using the following equation: (OD value/control OD value) ×100%.

RNA isolation and Real time-PCR analysis

Total RNA from astrocytes and brain tissues isolated using Trizol reagent (Roche, Basel, Switzerland), and complementary DNA (cDNA) were obtained after reverse transcription (Prime Script RT Reagent Kit, Takara, Tokyo, Japan). Then Real time-PCR reactions were performed as follows: incubation at 50 °C for 2 min, denaturing at 95 °C for 10 min, followed by 40 cycles of 95 °C for 15 sec, and 60 °C for 1 min.

Primers were designed by Sangon Biotech (Shanghai, China) and the PCR primer sequence for each gene was provided in Table 1.

Table 1 Sequences of primers

Primer sequence (5’-3’)	Product size (bp)	GenBank accession number
BDNF		
Forward, GCGGCAGATCCCCCGACTGC	496	M61175
Reverse, AAGTTGTGCGCAAATGACTG		
IGF-1		
Forward, GACCTGCTGGCAATAGCTTC	468	NM021578
Reverse, GACTGGCGAGCCTTAGTTTG		
VEGF		
Forward, GTGACAAGCCAAGGCGGTGAG	113	NM_001287114.1
Reverse, GATGGTGGTGTGGTGGTGACATG		
TGF-β		
Forward, GACCTGCTGGCAATAGCTTC	468	NM021578
Reverse, GACTGGCGAGCCTTAGTTTG		
Serping1		
Forward, GCGTCTTCCTCCACAGCCATTC	105	NM_012620.1
Reverse, TGTCTCTGTTGGATTGTGCCGAAC		
Rt1-s3		
Forward, AGCCTTCTCCATTCACCGACTCC	128	XM_006255917.3
Reverse, TCTCTTCCTCCTCCTCACAACAGC		
Psmb8		
Forward, TCATCGTGGCGGTGGACTCC	125	NM_080767.2
Reverse, CTGACAGTCGGCTGCACAACC		
Clcf1		
Forward, GTGTCATGGCAACTCTTGGCTACC	99	NM_207615.2
Reverse, TCTTCTGGAGGAAGTCGCTGTGG		
Tgm1		
Forward, GAGCCAGAGCCAGAGCCAGAG	96	XM_008770691.2
Reverse, GCAGGAGCAGCAGCCACAAC		
Ptgs2		
Forward, CGGACTGGATTCTACGGTGA	113	NM_017232.3
Reverse, CCCTTGAAGTGGGTCAGGAT		
Cd14		
Forward, CCCAAGCACACTCACTCAAC	106	XM_006254603.3
Reverse, ATCAGTCCTTTCTCGCCCAA		
Cd109		
Forward, GGCATGTTCCTGAACTCCTTCGC	119	NM_001108771.2
Reverse, CGCTCGGAATACTCTTGAGTGTCG		
S100α10		
Forward, ACCTGGACCAGTGCCGAGATG	128	NM_031114.1
Reverse, GCTCCAGTTGGCCTACTTCTTCTG		
GAPDH		
Forward, AGACAGCCGCATCTTCTTGT	323	X02231
Reverse, TACTCAGCACCAGCATCACC		
Thbs1		

Forward, GAGGAGGAGTACAGAGACGTAGCC Reverse, TTCCGTCACATCACCAACACAGTC FGF21	86	NM_001013062.1
Forward, CGACTGCTGCTGGCTGTCTTC Reverse, GGCTTCAGTGTCTTGGTCGTCATC β-actin	135	NM_020013.4
Forward, CACTGCAAACGGGGAAATGG Reverse, TGAGATGGACTGTCGGATGG	157	V01217

High-throughput gene sequencing

Three harvested vehicle- or rhFGF21-treated astrocyte samples from each group were subjected to high-throughput gene sequencing by Sangon Biotech (Shanghai, China). Briefly, total RNA was isolated using a Total RNA Extraction Kit, and a Qubit RNA Assay Kit and a Qubit 2.0 Fluorometer (Life Technologies, CA, USA) were used to measure the purity, concentration, and integrity of the RNA. Then, 0.1-1 μg of the total RNA was used as input material, and a VAHTSTM mRNA-seq V2 Library Prep Kit for Illumina® was used to generate sequencing libraries. PCR amplification and mRNA sequencing library construction were performed with fragmented mRNA. After the library quality was evaluated, mRNA sequencing was performed and sequencing reports generated by Sangon Biotech (Shanghai, China).

Statistical analysis

All value analysis was presented as the mean ± SEM of at least three independent experiments, and were performed using GraphPad Prism 7.0 (GraphPad Software Inc., San Diego, CA, USA). Two-way ANOVA for more than two groups. One-way ANOVA followed by Tukey’s tests when analyzing more than two groups. Non-paired Student's t-test was used for the comparisons of two groups. A value of $P<0.05$ was considered statistically significant.

Results

Ischemia induces FGF21 expression by microglia in the cortical area

The levels of endogenous FGF21 in the brain at different time points after MCAO/reperfusion were tested. We discovered that the mRNA levels of FGF21 were mainly concentrated in the cortical area but that FGF21 levels in the striatum significantly increased at 14 d after MCAO/reperfusion (Fig. 1a). In the cortical penumbras of mice subjected to MCAO/reperfusion, FGF21 protein levels increased and reached high levels from 1 d to 7 d before gradually declining to the levels found in the sham-operated mice over the next 7 d (Fig. 1b, c). Furthermore, compared with that in the contralateral cortex, the protein expression of FGF21 in the ipsilateral cortex was significantly elevated (by 2-fold) at 7 d (Fig. 1d, e). Moreover, immunohistochemistry further confirmed the increased FGF21 levels in ischemic cortices (Fig.

1f-i). Thus, 7 d after MCAO/reperfusion was selected as the optimal time point for the follow-up experiment.

Double-immunofluorescence staining of brain sections was performed to explore which types of cells were the main sources of endogenous FGF21 in ischemic cortices. The number of FGF21-immunoreactive puncta was greater in the ischemic core than in the boundary zone (Fig. 1j, k). FGF21-positive puncta were largely colocalized with Iba1-marked microglia, while few NeuN-positive neurons and GFAP-positive astrocytes were observed in the ischemic core (Fig. 1j). Additionally, some FGF21 was observed in microglia and astrocytes in the boundary zone (Fig. 1k).

Next, primary neuron, astrocyte and microglia cultures were subjected to OGD/R, and FGF21 protein expression was detected *in vitro*. As anticipated, Western blotting showed that FGF21 expression was extremely upregulated (by 5-fold) in microglia after 30 min of OGD and 24 h of reoxygenation (Fig. 1l, m). In contrast, FGF21 expression was not induced in the neuron or astrocyte cultures (Fig. 1l). Thus, our data strongly suggested that ischemia induced FGF21 generation by microglia in ischemic cortices.

FGF21 deficiency increases brain atrophy and aggravates neurological deficits

Given the amelioration of brain atrophy after administration of exogenous rhFGF21 [33], we hypothesized that endogenous FGF21 was capable of attenuating neurological deficits. There were no differences in appearance between wild-type (WT) and FGF21 KO mice (Fig. 2a). Determination of the cerebral infarct volume by TTC staining did not reveal any differences caused by the absence of FGF21 at 3 d after ischemia (Fig. 2b, c). However, FGF21-deficient mice exhibited larger residual brain volumes than WT mice at 14 d after MCAO/reperfusion (Fig. 2d, e). These findings verified that endogenous FGF21 could not attenuate the brain infarct volume during the acute stage of stroke but could ameliorate neuronal tissue loss over the long term.

Moreover, successive functional recovery of the brain after rhFGF21 treatment has previously been reported in a neonatal cerebral hypoxia/ischemia model [33], so we subsequently determined whether FGF21 deficiency induced detrimental functional outcomes. A battery of neurobehavioral tests was carried out during both the early and late periods of MCAO/reperfusion. As shown in Figure 2f, g and i, the sensorimotor outcomes were similar between WT and FGF21 KO mice during the acute stage; however, protracted deterioration was observed in FGF21 KO mice from 7 d to 14 d after ischemic injury. The latency to walk on a rotarod was greater in FGF21 KO mice than in WT mice, and the results for forelimb strength were the same as those for rotarod walking latency (Fig. 2f, g). Similarly, a corner-turning test suggested delayed recovery of FGF21 KO mice compared with WT mice during the late stage (Fig. 2i). However, FGF21 KO mice exhibited much worse outcomes than WT mice during the early stage in the modified neurological severity score (mNSS) test (Fig. 2h). Collectively, the behavioral assay data demonstrated that the absence of FGF21 led to persistent impairment of neurological function at late stages after ischemic injury.

rhFGF21-mediated astrocytes contribute to neuronal survival and upregulate synaptic protein expression

FGF21 attenuates neuronal apoptosis in the penumbra after MCAO/reperfusion through the FGFR1/PI3K/caspase-3 signaling pathway [37]. Here, we investigated whether FGF21 also promotes beneficial neuronal outcomes by mediating glial activity. After we treated astrocytes with rhFGF21 (100 nM), we transferred the conditioned medium to OGD-induced neurons (Fig. 3a). There were no visible morphological changes in neurons after treatment with the conditioned medium or with rhFGF21 alone (Fig. 3b). Notably, these media were protective; in particular, the conditioned medium from rhFGF21-treated astrocytes could protect neurons against OGD. In addition, normal neuronal viability gradually decreased by 40% after 2 h of OGD and 24 h of reoxygenation (Fig. 3c); however, rhFGF21-treated astrocyte conditioned medium (21ACM) effectively increased neuronal viability (Fig. 3c). rhFGF21 alone also exhibited a protective effect against OGD-induced neuronal death (Fig. 3a).

In addition, we hypothesized that conditioned medium from astrocytes would promote synaptic remodeling of neurons, and the results of presynaptic and postsynaptic expression assessment were similar to those of neuronal viability assessment. As shown in Figure 3e and f, the expression levels of synaptotagmin 1 (SYT1) and synaptophysin after OGD/R onset were significantly promoted in the normal astrocyte conditioned medium (ACM)- and 21ACM-treated neurons compared with control neurons, but rhFGF21-activated astrocytes exhibited upregulated postsynaptic density 95 (PSD95) expression (Fig. 3d). In addition, treatment with rhFGF21 alone was as effective as treatment with 21ACM in upregulating synaptic protein expression after OGD/R (Fig. 3d-f). All these results proved the beneficial effects of rhFGF21-treated astrocytes on neuronal survival and neuroplasticity.

rhFGF21 actives astrocytes and modulates the astrocytic phenotype

The above cellular findings verified that rhFGF21 could attenuate neuronal damage by influencing astrocytes. However, the mechanism of this effect on astrocytes remained unclear; thus, we examined the effect of rhFGF21 on astrocyte physiology. When astrocytes were treated with rhFGF21 for 24 h, the morphology and cellular viability did not change (Fig. 4a, b). Then, gene sequencing was performed, and the gene expression profiles of the astrocytes in the Norm and rhFGF21 groups were compared. The differentially expressed genes between the Norm and rhFGF21 groups are delineated in a volcano plot (Fig. 4c). A total of 2380 differentially expressed genes were detected by gene sequencing bioinformatic analyses, of which 1350 genes were upregulated and 1030 genes were downregulated in the rhFGF21 group. A Venn diagram was used to visually demonstrate the numbers of expressed genes in the different groups as well as the overlapping expression relationships (Fig. 4d). The overlapping region represents the expressed genes (18448) that were shared between the two groups. In addition, gene expression pattern clustering analysis of genes with significant differences was employed to discover commonalities in the expression of different genes (Fig. 4e).

To further assess astrocyte reactivity, a heatmap of the reactive transcripts was utilized to determine gene expression differences in astrocytes between the Norm and rhFGF21 groups (Fig. 4f). Treatment with rhFGF21 strongly induced astrocytic activation by upregulating Lcn2, Steap4 and Cxcl10 as well as the prototypic A2 genes Clcf1, Ptx3, Ptgs2, and Cd14 (Fig. 4f). Under these experimental conditions, rhFGF21

also altered the expression of A1 phenotype genes, such as Serping1, Gbp2, Fbln5 and Psmb8 (Fig. 4f). Then, RT-PCR was performed to confirm the induction of several phenotypic markers. rhFGF21 effectively induced the expression of Tgm1, Cd109 and S100α10, but not Clcf1, Ptgs2 or Cd14 (Fig. 4g). In addition, the mRNA levels of A1 markers (Serping1, Rt1-s3 and Psmb8) were decreased by rhFGF21 (Fig. 4g).

rhFGF21 upregulates astrocyte-induced expression of trophic factors

As Christopherson *et al* previously described, A2 astrocytes induce synaptogenesis by secreting several trophic proteins [38]. After establishing that rhFGF21 altered A2 gene expression in astrocytes, we sought to investigate the changes in key factors released by rhFGF21-activated astrocytes. As shown in the heatmap of the reactive transcripts, the production of trophic factors such as BDNF, transforming growth factor-β (TGF-β), FGF2, and thrombospondin-1 (Thbs1) was markedly increased by rhFGF21 treatment (Fig. 5a). Subsequently, elevated mRNA levels of BDNF, Thbs1 and TGF-β were observed, whereas IGF-1 and vascular endothelial growth factor (VEGF) mRNA expression was not changed (Fig. 5b). Similarly, the protein levels of TGF-β, BDNF and Thbs-1 were upregulated after treatment with rhFGF21 for 24 h, while those of VEGF and IGF-1 were not altered (Fig. 5c, d). Taken together, these data revealed that rhFGF21 guided astrocytes into potentially beneficial phenotypes that are expected to accelerate neurobehavioral recovery by producing neurotrophic factors.

rhFGF21 modulates the astrocytic phenotype and upregulates trophic factors *in vivo*

The above evidence suggested that rhFGF21 promoted astrocytes activation thereby contributed to the protection of neurons from OGD injury. Therefore, we next sought to explore whether rhFGF21 was associated with astrocytic phenotype shifts in an animal model of ischemic stroke. When the mice were subjected to MCAO/reperfusion, rhFGF21 were administered intraperitoneal after the arterial occlusion, and then RT-PCR was used to analyze the astrocytic phenotype gene expression change in ipsilateral brain cortex at 7 d after ischemia. We found that several A1 and A2 phenotype genes (Psmb8, Clcf1, Tgm1 and Cd109) expression increased after MCAO/reperfusion (Fig. 6a). Meaningfully, there was a significant increase in the expression of A2 markers (Clcf1, Tgm1, Pptgs2, Cd109 and S100α10) after rhFGF21 treatment, while rhFGF21 also induced Serping1, Rt1-s3 and Psmb8, prototypic A2 genes (Fig. 6a).

One of the central roles of A2 astrocytes-derived BDNF and Thbs1 in the ischemic brain is to protect brain cells *via* promoting synaptogenesis [39]. After establishing that rhFGF21 can alter gene expression in astrocytes, we next examined rhFGF21 could enhance the production of BDNF and Thbs1 in the brain. As shown in Fig 6 b and c, the protein levels of BDNF and Thbs1 were significantly higher in the rhFGF21 group than those in the Sham and MCAO groups at 7 d after ischemia injury (Fig. 6b, c).

Discussion

FGF21, which has been recognized as a prime lipid catabolic factor, plays an important role in regulating energy balance [20]. In recent years, it has been found that FGF21 could be an early biomarker for

dysregulated mitochondrial dynamics and endoplasmic reticulum (ER) stress conditions and that it induces glial cells to promote remyelination in response to CNS disorders [40, 41]. Following cerebral ischemia/reperfusion injury in rats, endogenous FGF21 production by neurons in the penumbra is effectively increased [37]. Consistent with this information, prolonged increases in the mRNA and protein levels of FGF21 in ischemic cortices were observed from days 1 to 7 after MCAO/reperfusion in the current study, suggesting an emergency response to brain ischemia. At 7 d after MCAO/reperfusion, FGF21-positive puncta were mainly localized in Iba1-positive microglial cells *in vivo*, and *in vitro*, microglia, but not neurons or astrocytes, significantly expressed FGF21 in response to OGD/R, identifying microglia as the sources of FGF21 in ischemic brain tissue. These data further support the suggestion by Salminen *et al* that endogenous FGF21 is released by different cell types after different degrees of brain damage to alleviate related tissue injury [42].

It has been reported that FGF21 reduces caspase-3 activity and cell death by activating the PI3K/Akt/Bcl-2-dependent cell death signaling cascade [43]. For example, Ye *et al* reported that exogenous FGF21 treatment can inhibit neuronal apoptosis by regulating the PI3K/Akt signaling pathway to ameliorate brain injury [33]. In addition, administration of exogenous FGF21 downregulates ER stress-related protein expression by activating the ERK1/2, PI3K/Akt, and JNK signaling pathways, thus protecting neurons from ischemic injury [44]. Consistent with these findings, we have demonstrated a role for endogenous FGF21 in brain tissue recovery and functional outcome improvement after stroke. A greater extent of neuronal tissue loss was observed in FGF21 KO mice than in WT mice at 14 d after MCAO/reperfusion, but TTC staining showed no significant difference in infarct volume between FGF21 KO mice and WT mice at the early stage after surgery. Furthermore, FGF21 deficiency significantly prolonged motor deficits and results in degeneration of long-term behavioral performance after ischemia. On the other hand, FGF21 has been reported to ameliorate cognitive functioning in rats after hypoxic/ischemic brain injury [33]. However, the effects of endogenous FGF21 on cognitive performance need further exploration in a future study. The present data strongly suggest that FGF21 stably promotes long-term neurological recovery; thus, targeting of FGF21 is a promising therapeutic strategy after stroke.

In response to brain damage, microglia are capable of producing neurotrophic and anti-inflammatory cytokines, such as IL-10, IL-4, IGF-1 and TGF-β, that help inhibit inflammation and promote tissue repair during the late stage [45]. Here, we have demonstrated that microglial-derived FGF21 is a beneficial signal that delays neuronal death and reduces brain atrophy over the long term. Additionally, TNF, IL-1α, and IL-6 released by lipopolysaccharide (LPS)-activated microglia are together sufficient to induce the A1 phenotype in astrocytes [46, 47]. However, studies on A2 phenotype modulation in astrocytes are still rarely reported. We hypothesized that FGF21 from activated microglia participates in astrocytic phenotype modulation. Consistent with this hypothesis, we observed an A2 phenotype shifts after rhFGF21 treatment in the current study, and we found that the levels of A1-like markers such as Serping1, Rt1-s3, and Psmb8 were decreased. Thus, our data clearly show that rhFGF21 induces the A2 phenotype, and the observed reduction in the A1 phenotype strongly supports the contribution of rhFGF21 to astrocyte modulation in astrocyte cultures and ischemic brain. Furthermore, A2 astrocytes are now known to play beneficial roles in neuronal survival under pathological conditions [48, 13]. After brain damage, A2

astrocytes promote synapse formation, support blood-brain barrier function, and release nutritional factors such as BDNF, Thbs-1, and IGF-1, which have been suggested to be protective in models of stroke [49]. BDNF produced by rhFGF21-activated astrocytes is well known to play extremely important roles in the CNS, contributing to neuronal survival as well as the maintenance of homeostatic neuroplasticity [50]. Astrocytic release of high Thbs-1 levels can enhance synaptic and dendritic plasticity [51]. Our results confirm these findings, as conditioned media from astrocytes containing these trophic factors supported the survival of neurons and helped with neuroplasticity.

Our current study focused on the effects of rhFGF21 on astrocyte phenotype under normal or pathological conditions. However, in the context of CNS disease, activated microglia not only exhibit a protective phenotype but also produce the inflammatory cytokines IL-6, IL-1β and TNF-α, the collective effects of FGF21 and circulating factors on astrocyte modulation warrant further investigation [5].

Conclusions

In summary, our study has illustrated, for the first time, that FGF21 is mainly produced by microglia in response to ischemia. Under conditions simulating ischemia, FGF21 attenuated brain tissue loss and stabilized behavioral outcomes during the recovery phase. Subsequently, FGF21 also mediated the astrocytic phenotype and upregulated astrocytic expression of neurotrophic factors. Finally, FGF21 stimulated trophic factor production via astrocyte modulation, promoting neuroprotection and neuroplasticity in OGD/R-induced neurons. These findings will contribute to the use of FGF21 as a promising agent for stroke treatment.

Abbreviations

FGF21: Fibroblast growth factor 21; CNS: central nervous system; MCAO: middle cerebral artery occlusion; CCA: common carotid artery; ICA: internal carotid artery; ECA: external carotid artery; MCA: middle cerebral artery; CBF: cerebral blood flow; OGD: oxygen/glucose deprivation; TTC: 2,3,5-triphenyltetrazolium chloride; H&E: hematoxylin-eosin; CCK-8: cell counting kit-8; rt-PA: recombinant tissue-type plasminogen activator; BDNF: brain-derived neurotropic factor; IGF-1: insulin-like growth factor 1; NAMPT: nicotinamide phosphoribosyl transferase; 21ACM: rhFGF21-treated astrocyte conditioned medium; ACM: normal astrocyte conditioned medium; SYT1: synaptotagmin1; PSD95: postsynaptic density 95; TGF-β: transforming growth factor-β; Thbs1: thrombospondin-1; VEGF: vascular endothelial growth factor; ER: endoplasmic reticulum; LPS: lipopolysaccharide; WT: wild type; KO: knock-out

Declarations

Acknowledgement

The authors want to thank Chinese-American Research Institute for Diabetic Complications (Wenzhou, Zhejiang, China) for supplying FGF21 knockout mice.

Authors' contributions

FL, XW and LL conceived and designed the study. FL, JD and PL performed research. DW and LZ analyzed and interpreted data. FL and PW wrote the paper. All authors approved the final submitted version. All authors read and approved the final manuscript.

Funding

This work was supported by National Natural Science Foundation of China (Grant number 81771284, 81971180), Public Welfare Technology Application Research Foundation of Zhejiang Province (Grant number 2017C33080), and Wenzhou Municipal Science and Technology Bureau Project (Grant number ZY2019001).

Availability of data and materials

All data generated or analysed during this study are included in this published article and its supplementary information files.

Ethics approval and consent to participate

All animal procedures used in this study were conducted in strict compliance with The National Institute of Health Guide for Use and Care of Laboratory Animals and the Animal Ethics Committee of Wenzhou Medical University, China, approved all experiments. This article does not contain any studies with human participants performed by any of the authors.

Consent for publication

All authors have read the manuscript and approved the final version.

Declaration of Competing Interests

The authors declare that they have no competing interests.

References

1. Doyle KP, Simon RP, Stenzel-Poore MP. Mechanisms of ischemic brain damage. Neuropharmacology. 2008;55(3):310-8. doi:10.1016/j.neuropharm.2008.01.005.

2. White BC, Sullivan JM, DeGracia DJ, O'Neil BJ, Neumar RW, Grossman LI et al. Brain ischemia and reperfusion: molecular mechanisms of neuronal injury. J Neurol Sci. 2000;179(S 1-2):1-33. doi:10.1016/s0022-510x(00)00386-5.

3. Alexandrov AV. Current and future recanalization strategies for acute ischemic stroke. J Intern Med. 2010;267(2):209-19. doi:10.1111/j.1365-2796.2009.02206.x.

4. Cheng H, Huang SS, Lin SM, Lin MJ, Chu YC, Chih CL et al. The neuroprotective effect of glial cell line-derived neurotrophic factor in fibrin glue against chronic focal cerebral ischemia in conscious rats. Brain Res. 2005;1033(1):28-33. doi:10.1016/j.brainres.2004.10.067.

5. Nedergaard M, Dirnagl U. Role of glial cells in cerebral ischemia. Glia. 2005;50(4):281-6. doi:10.1002/glia.20205.

6. Javidi E, Magnus T. Autoimmunity After Ischemic Stroke and Brain Injury. Front Immunol. 2019;10:686. doi:10.3389/fimmu.2019.00686.

7. Esenwa CC, Elkind MS. Inflammatory risk factors, biomarkers and associated therapy in ischaemic stroke. Nat Rev Neurol. 2016;12(10):594-604. doi:10.1038/nrneurol.2016.125.

8. Chen D, Dixon BJ, Doycheva DM, Li B, Zhang Y, Hu Q et al. IRE1alpha inhibition decreased TXNIP/NLRP3 inflammasome activation through miR-17-5p after neonatal hypoxic-ischemic brain injury in rats. J Neuroinflammation. 2018;15(1):32. doi:10.1186/s12974-018-1077-9.

9. Trettel F, Di Castro MA, Limatola C. Chemokines: Key Molecules that Orchestrate Communication among Neurons, Microglia and Astrocytes to Preserve Brain Function. Neuroscience. 2019. doi:10.1016/j.neuroscience.2019.07.035.

10. Perez-de Puig I, Miro F, Salas-Perdomo A, Bonfill-Teixidor E, Ferrer-Ferrer M, Marquez-Kisinousky L et al. IL-10 deficiency exacerbates the brain inflammatory response to permanent ischemia without preventing resolution of the lesion. J Cereb Blood Flow Metab. 2013;33(12):1955-66. doi:10.1038/jcbfm.2013.155.

11. Ma Y, Wang J, Wang Y, Yang GY. The biphasic function of microglia in ischemic stroke. Prog Neurobiol. 2017;157:247-72. doi:10.1016/j.pneurobio.2016.01.005.

12. Chen F, Weng Z, Xia Q, Cao C, Leak RK, Han L et al. Intracerebroventricular Delivery of Recombinant NAMPT Deters Inflammation and Protects Against Cerebral Ischemia. Transl Stroke Res. 2019;10(6):719-28. doi:10.1007/s12975-019-00692-0.

13. Su Y, Chen Z, Du H, Liu R, Wang W, Li H et al. Silencing miR-21 induces polarization of astrocytes to the A2 phenotype and improves the formation of synapses by targeting glypican 6 via the signal transducer and activator of transcription-3 pathway after acute ischemic spinal cord injury. FASEB J. 2019:fj201900743R. doi:10.1096/fj.201900743R.

14. Sofroniew MV, Vinters HV. Astrocytes: biology and pathology. Acta Neuropathol. 2010;119(1):7-35. doi:10.1007/s00401-009-0619-8.

15. Alonso G. NG2 proteoglycan-expressing cells of the adult rat brain: possible involvement in the formation of glial scar astrocytes following stab wound. Glia. 2005;49(3):318-38. doi:10.1002/glia.20121.

16. Peng L, Zhao Y, Li Y, Zhou Y, Li L, Lei S et al. Effect of DJ-1 on the neuroprotection of astrocytes subjected to cerebral ischemia/reperfusion injury. Journal of Molecular Medicine. 2018;97(2):189-99. doi:10.1007/s00109-018-1719-5.

17. Chung WS, Clarke LE, Wang GX, Stafford BK, Sher A, Chakraborty C et al. Astrocytes mediate synapse elimination through MEGF10 and MERTK pathways. Nature. 2013;504(7480):394-400. doi:10.1038/nature12776.

18. Li YH, Fu HL, Tian ML, Wang YQ, Chen W, Cai LL et al. Neuron-derived FGF10 ameliorates cerebral ischemia injury via inhibiting NF-kappaB-dependent neuroinflammation and activating PI3K/Akt survival signaling pathway in mice. Sci Rep. 2016;6:19869. doi:10.1038/srep19869.

19. Nakamura K, Arimura K, Nishimura A, Tachibana M, Yoshikawa Y, Makihara N et al. Possible involvement of basic FGF in the upregulation of PDGFRbeta in pericytes after ischemic stroke. Brain Res. 2016;1630:98-108. doi:10.1016/j.brainres.2015.11.003.

20. Li X. The FGF metabolic axis. Front Med. 2019. doi:10.1007/s11684-019-0711-y.

21. Kruse R, Vienberg SG, Vind BF, Andersen B, Hojlund K. Effects of insulin and exercise training on FGF21, its receptors and target genes in obesity and type 2 diabetes. Diabetologia. 2017;60(10):2042-51. doi:10.1007/s00125-017-4373-5.

22. Cong WT, Ling J, Tian HS, Ling R, Wang Y, Huang BB et al. Proteomic study on the protective mechanism of fibroblast growth factor 21 to ischemia-reperfusion injury. Can J Physiol Pharmacol. 2013;91(11):973-84. doi:10.1139/cjpp-2012-0441.

23. Liang P, Zhong L, Gong L, Wang J, Zhu Y, Liu W et al. Fibroblast growth factor 21 protects rat cardiomyocytes from endoplasmic reticulum stress by promoting the fibroblast growth factor receptor 1-extracellular signalregulated kinase 1/2 signaling pathway. Int J Mol Med. 2017;40(5):1477-85. doi:10.3892/ijmm.2017.3140.

24. Makela J, Tselykh TV, Maiorana F, Eriksson O, Do HT, Mudo G et al. Fibroblast growth factor-21 enhances mitochondrial functions and increases the activity of PGC-1alpha in human dopaminergic neurons via Sirtuin-1. Springerplus. 2014;3:2. doi:10.1186/2193-1801-3-2.

25. Taliyan R, K CS, Kakoty V. Therapeutic approaches to Alzheimer's type of dementia: A focus on FGF21 mediated neuroprotection. Curr Pharm Des. 2019. doi:10.2174/1381612825666190716101411.

26. Chen J, Hu J, Liu H, Xiong Y, Zou Y, Huang W et al. FGF21 Protects the Blood-Brain Barrier by Upregulating PPARgamma via FGFR1/beta-klotho after Traumatic Brain Injury. J Neurotrauma. 2018;35(17):2091-103. doi:10.1089/neu.2017.5271.

27. Zhao X, Wang H, Sun G, Zhang J, Edwards NJ, Aronowski J. Neuronal Interleukin-4 as a Modulator of Microglial Pathways and Ischemic Brain Damage. J Neurosci. 2015;35(32):11281-91.

doi:10.1523/JNEUROSCI.1685-15.2015.

28. Mao L, Jia J, Zhou X, Xiao Y, Wang Y, Mao X et al. Delayed administration of a PTEN inhibitor BPV improves functional recovery after experimental stroke. Neuroscience. 2013;231:272-81. doi:10.1016/j.neuroscience.2012.11.050.

29. Zhang L, Schallert T, Zhang ZG, Jiang Q, Arniego P, Li Q et al. A test for detecting long-term sensorimotor dysfunction in the mouse after focal cerebral ischemia. J Neurosci Methods. 2002;117(2):207-14.

30. Meyer OA, Tilson HA, Byrd WC, Riley MT. A method for the routine assessment of fore- and hindlimb grip strength of rats and mice. Neurobehav Toxicol. 1979;1(3):233-6.

31. Lee JK, Kim JE, Sivula M, Strittmatter SM. Nogo receptor antagonism promotes stroke recovery by enhancing axonal plasticity. J Neurosci. 2004;24(27):6209-17. doi:10.1523/JNEUROSCI.1643-04.2004.

32. Liu H, Zhao Y, Zou Y, Huang W, Zhu L, Liu F et al. Heparin-poloxamer hydrogel-encapsulated rhFGF21 enhances wound healing in diabetic mice. FASEB J. 2019;33(9):9858-70. doi:10.1096/fj.201802600RR.

33. Ye L, Wang X, Cai C, Zeng S, Bai J, Guo K et al. FGF21 promotes functional recovery after hypoxic-ischemic brain injury in neonatal rats by activating the PI3K/Akt signaling pathway via FGFR1/beta-klotho. Exp Neurol. 2019;317:34-50. doi:10.1016/j.expneurol.2019.02.013.

34. Mo JL, Liu Q, Kou ZW, Wu KW, Yang P, Chen XH et al. MicroRNA-365 modulates astrocyte conversion into neuron in adult rat brain after stroke by targeting Pax6. Glia. 2018;66(7):1346-62. doi:10.1002/glia.23308.

35. Lin L, Desai R, Wang X, Lo EH, Xing C. Characteristics of primary rat microglia isolated from mixed cultures using two different methods. J Neuroinflammation. 2017;14(1):101. doi:10.1186/s12974-017-0877-7.

36. Lin L, Wang Q, Qian K, Cao Z, Xiao J, Wang X et al. bFGF Protects Against Oxygen Glucose Deprivation/Reoxygenation-Induced Endothelial Monolayer Permeability via S1PR1-Dependent Mechanisms. Mol Neurobiol. 2018;55(4):3131-42. doi:10.1007/s12035-017-0544-0.

37. Zheng W, Matei N, Pang J, Luo X, Song Z, Tang J et al. Delayed recanalization at 3 days after permanent MCAO attenuates neuronal apoptosis through FGF21/FGFR1/PI3K/Caspase-3 pathway in rats. Exp Neurol. 2019;320:113007. doi:10.1016/j.expneurol.2019.113007.

38. Christopherson KS, Ullian EM, Stokes CC, Mullowney CE, Hell JW, Agah A et al. Thrombospondins are astrocyte-secreted proteins that promote CNS synaptogenesis. Cell. 2005;120(3):421-33. doi:10.1016/j.cell.2004.12.020.

39. Zhou L, Lin Q, Wang P, Yao L, Leong K, Tan Z et al. Enhanced neuroprotective efficacy of bone marrow mesenchymal stem cells co-overexpressing BDNF and VEGF in a rat model of cardiac arrest-induced global cerebral ischemia. Cell Death Dis. 2017;8(5):e2774. doi:10.1038/cddis.2017.184.

40. Kuroda M, Muramatsu R, Maedera N, Koyama Y, Hamaguchi M, Fujimura H et al. Peripherally derived FGF21 promotes remyelination in the central nervous system. J Clin Invest. 2017;127(9):3496-509. doi:10.1172/JCI94337.

41. Restelli LM, Oettinghaus B, Halliday M, Agca C, Licci M, Sironi L et al. Neuronal Mitochondrial Dysfunction Activates the Integrated Stress Response to Induce Fibroblast Growth Factor 21. Cell Rep. 2018;24(6):1407-14. doi:10.1016/j.celrep.2018.07.023.

42. Salminen A, Kaarniranta K, Kauppinen A. Regulation of longevity by FGF21: Interaction between energy metabolism and stress responses. Ageing Res Rev. 2017;37:79-93. doi:10.1016/j.arr.2017.05.004.

43. Liu SQ, Roberts D, Kharitonenkov A, Zhang B, Hanson SM, Li YC et al. Endocrine protection of ischemic myocardium by FGF21 from the liver and adipose tissue. Sci Rep. 2013;3:2767. doi:10.1038/srep02767.

44. Yang X, Hui Q, Yu B, Huang Z, Zhou P, Wang P et al. Design and Evaluation of Lyophilized Fibroblast Growth Factor 21 and Its Protection against Ischemia Cerebral Injury. Bioconjug Chem. 2018;29(2):287-95. doi:10.1021/acs.bioconjchem.7b00588.

45. Otsuka S, Sakakima H, Sumizono M, Takada S, Terashi T, Yoshida Y. The neuroprotective effects of preconditioning exercise on brain damage and neurotrophic factors after focal brain ischemia in rats. Behav Brain Res. 2016;303:9-18. doi:10.1016/j.bbr.2016.01.049.

46. Liddelow SA, Guttenplan KA, Clarke LE, Bennett FC, Bohlen CJ, Schirmer L et al. Neurotoxic reactive astrocytes are induced by activated microglia. Nature. 2017;541(7638):481-7. doi:10.1038/nature21029.

47. Armstead WM, Hekierski H, Pastor P, Yarovoi S, Higazi AA, Cines DB. Release of IL-6 After Stroke Contributes to Impaired Cerebral Autoregulation and Hippocampal Neuronal Necrosis Through NMDA Receptor Activation and Upregulation of ET-1 and JNK. Transl Stroke Res. 2019;10(1):104-11. doi:10.1007/s12975-018-0617-z.

48. Chan SJ, Niu W, Hayakawa K, Hamanaka G, Wang X, Cheah PS et al. Promoting Neuro-Supportive Properties of Astrocytes with Epidermal Growth Factor Hydrogels. Stem Cells Transl Med. 2019. doi:10.1002/sctm.19-0159.

49. Wasilewski D, Priego N, Fustero-Torre C, Valiente M. Reactive Astrocytes in Brain Metastasis. Front Oncol. 2017;7:298. doi:10.3389/fonc.2017.00298.

50. Luo W, Liu T, Li S, Wen H, Zhou F, Zafonte R et al. The Serum BDNF Level Offers Minimum Predictive Value for Motor Function Recovery After Stroke. Transl Stroke Res. 2019;10(4):342-51.

doi:10.1007/s12975-018-0648-5.

51. Liauw J, Hoang S, Choi M, Eroglu C, Choi M, Sun GH et al. Thrombospondins 1 and 2 are necessary for synaptic plasticity and functional recovery after stroke. J Cereb Blood Flow Metab. 2008;28(10):1722-32. doi:10.1038/jcbfm.2008.65.

Figures

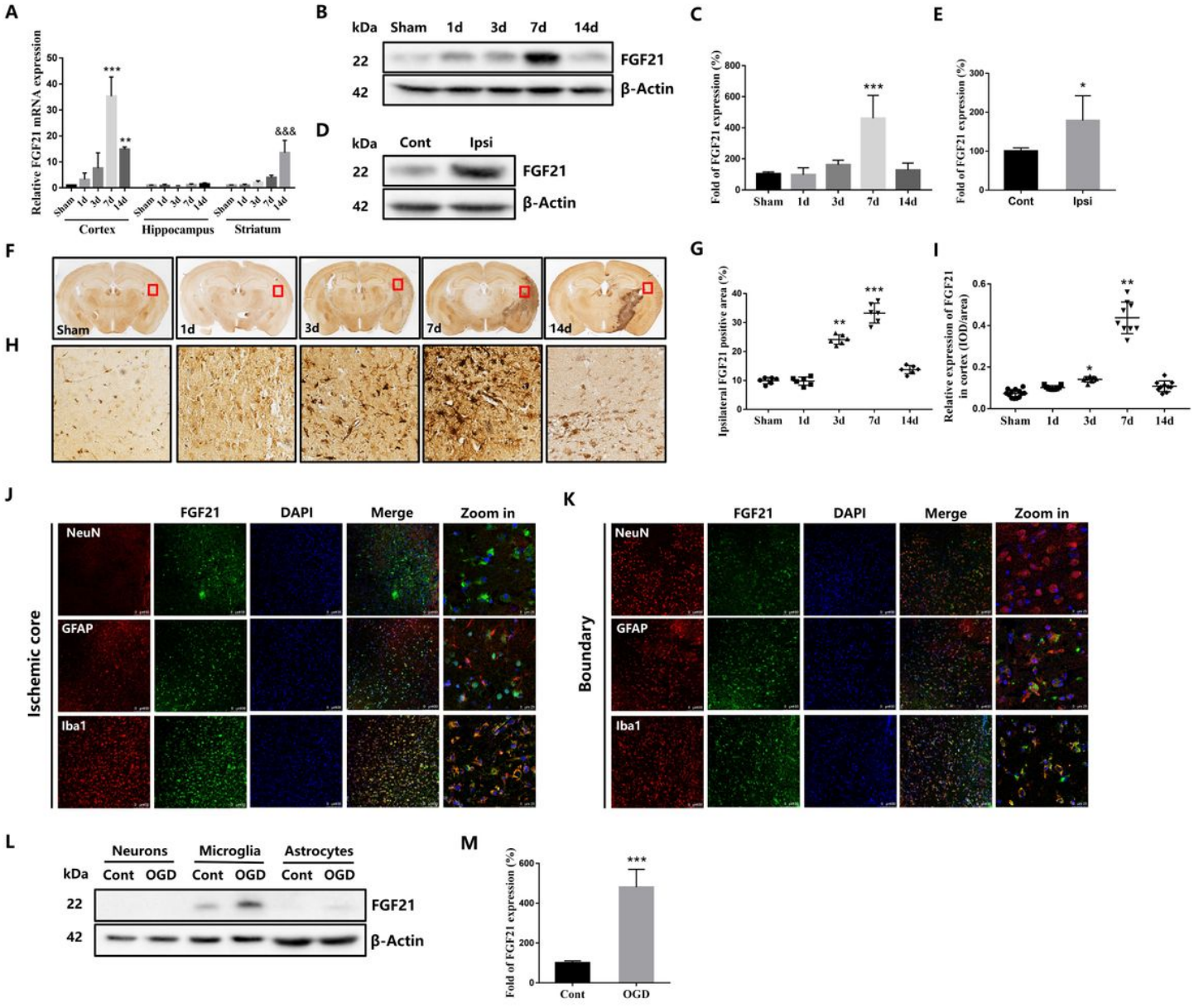

Figure 1

Induction of FGF21 expression in ischemic cortices. (A) FGF21 mRNA levels in ischemic cortices, hippocampi, and striata at 1, 3, 7, 14 d after transient MCAO/reperfusion. ***P<0.001 and **P<0.01 vs the sham group (Cortex), &&&P<0.001 vs the sham group (Striatum) (one-way ANOVA); n=6. (B and C) Representative Western blot images and quantification of FGF21 in the cortical penumbra. ***P<0.001 vs

the sham group (one-way ANOVA); n=8. (D and E) Representative Western blot images and quantification of FGF21 in the ipsilateral (Ipsi) cortical penumbra compared with the contralateral (Cont) cortical penumbra at 7 d after MCAO/reperfusion. *P<0.05 vs. the Cont group (t-test); n=5. (F) Representative images of immunohistochemical staining of FGF21. Scale bar = 1 mm. (G) Percentage quantification of the injured ipsilateral FGF21-positive area. **P<0.01 and ***P<0.001 vs the sham group (one-way ANOVA); n=6. (H) Magnified images of the cortical region. (I) Quantification of the average integrated optical density (IOD) of FGF21-positive staining in the cortical region. *P<0.05 and **P<0.01 vs the sham group (one-way ANOVA); n=7. IOD/area: IOD per stained area. (J and K) Representative double-immunofluorescence staining images of FGF21 (green), neurons (red, NeuN-positive), astrocytes (red, GFAP-positive) and microglia (red, Iba1-positive) in the ischemic core (J) and in the boundary zone (K). Scale bars = 100 μm and 25 μm. (L and M) Representative Western blot images and quantification of FGF21 in OGD/R-induced neurons, microglia (m) and astrocytes. ***P<0.001 vs the Cont group (t-test); n=5.

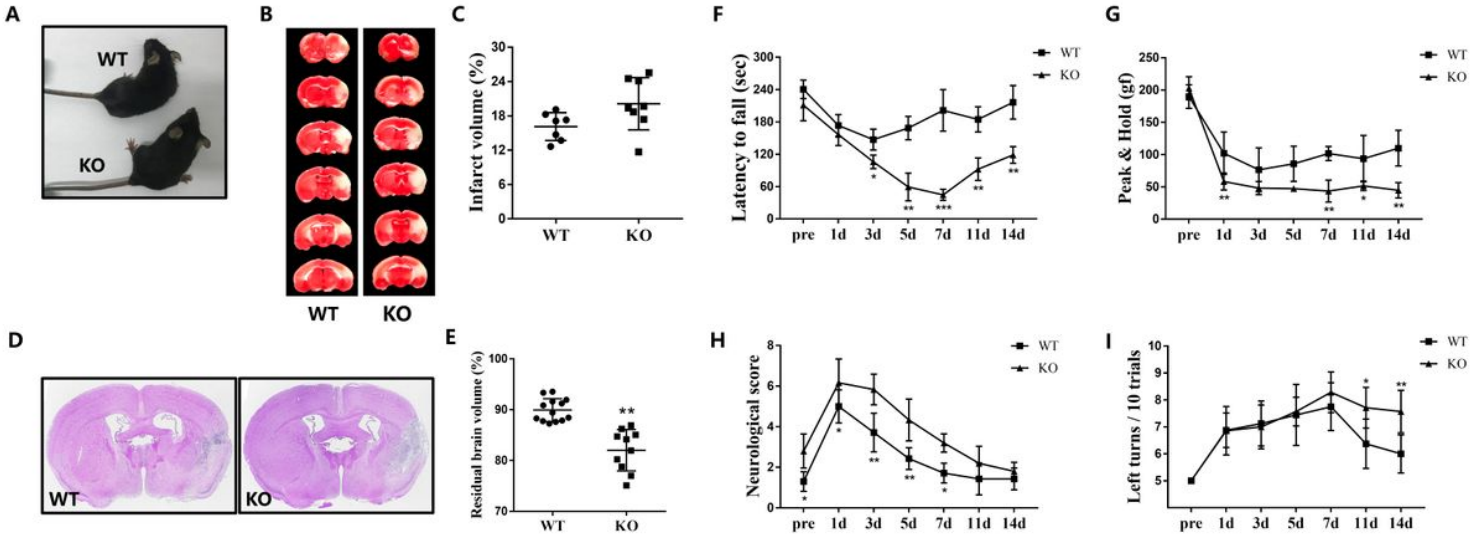

Figure 2

FGF21 deficiency exacerbates brain atrophy and neurological deficits. (A) Images showing the appearances of WT and FGF21 KO mice. (B) The infarct volumes of WT and FGF21 KO mice were assayed by TTC staining at 3 d after MCAO/reperfusion. Six brain sections were obtained from one mouse. (C) Quantification of the brain infarct volume. n=7. (D) The residual brain volumes of WT and FGF21 KO mice were determined at 14 d after MCAO/reperfusion by HE staining. (E) Quantification of brain atrophy by volume. **P<0.01 for the WT vs FGF21 KO group (t-test); n=13 for the WT group, and n=10 for the FGF21 KO group. (F-I) Neurological functions were evaluated with rotarod (F), grip strength (G), mNSS (H) and corner-turning (I) tests. *P<0.05, **P<0.01, and ***P<0.001 for the WT vs FGF21 KO group (t-test); n=9 for the sham group, n=9 for the WT group, and n=11 for the FGF21 KO group.

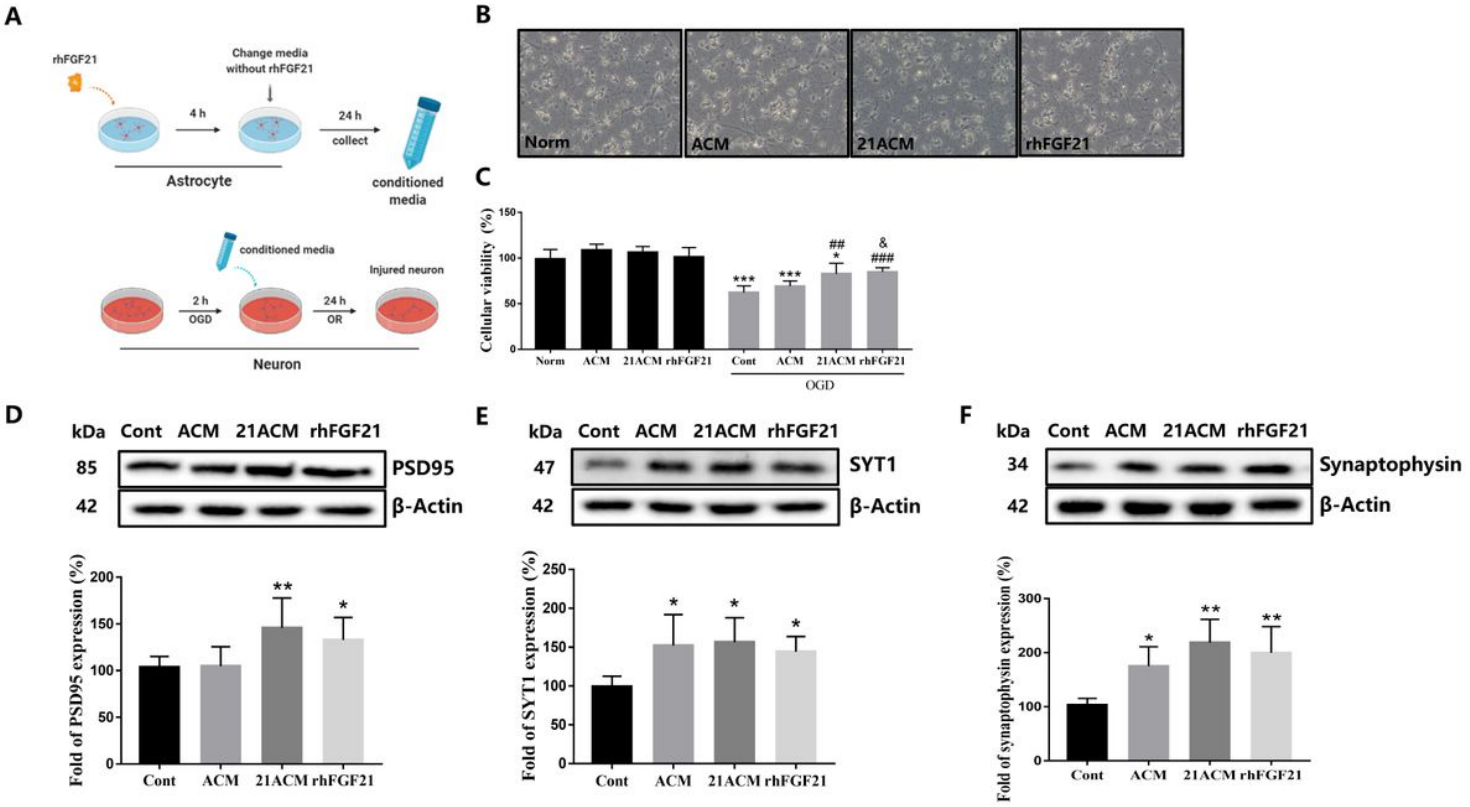

Figure 3

Effects of rhFGF21-mediated astrocytes on neuronal survival and neuroplasticity after OGD/R exposure. (A) A flow chart of the experiment with conditioned medium transfer from astrocytes to neurons in culture. (B) Images showing the morphology of cultured neurons after treatment with conditioned medium from astrocytes or with rhFGF21 alone. Norm, normal, nontreated neurons; ACM, conditioned medium from normal astrocytes; 21ACM, conditioned medium from rhFGF21-treated astrocytes; rhFGF21, rhFGF21 treatment alone. (C) Neuronal viability after conditioned medium treatment under normal or OGD/R conditions. *P<0.05 and ***P<0.001 vs the Norm group; ##P<0.05 and ###P<0.001 vs the Cont group; &P<0.05 vs the OGD/R-ACM group (one-way ANOVA); n=6. (D-F) Representative Western blot images and quantification of PSD95, SYT1, and synaptophysin levels in OGD/R-induced neurons cultured with conditioned medium. *P<0.05, **P<0.01, and ***P<0.001 vs the Cont group (one-way ANOVA); n=8.

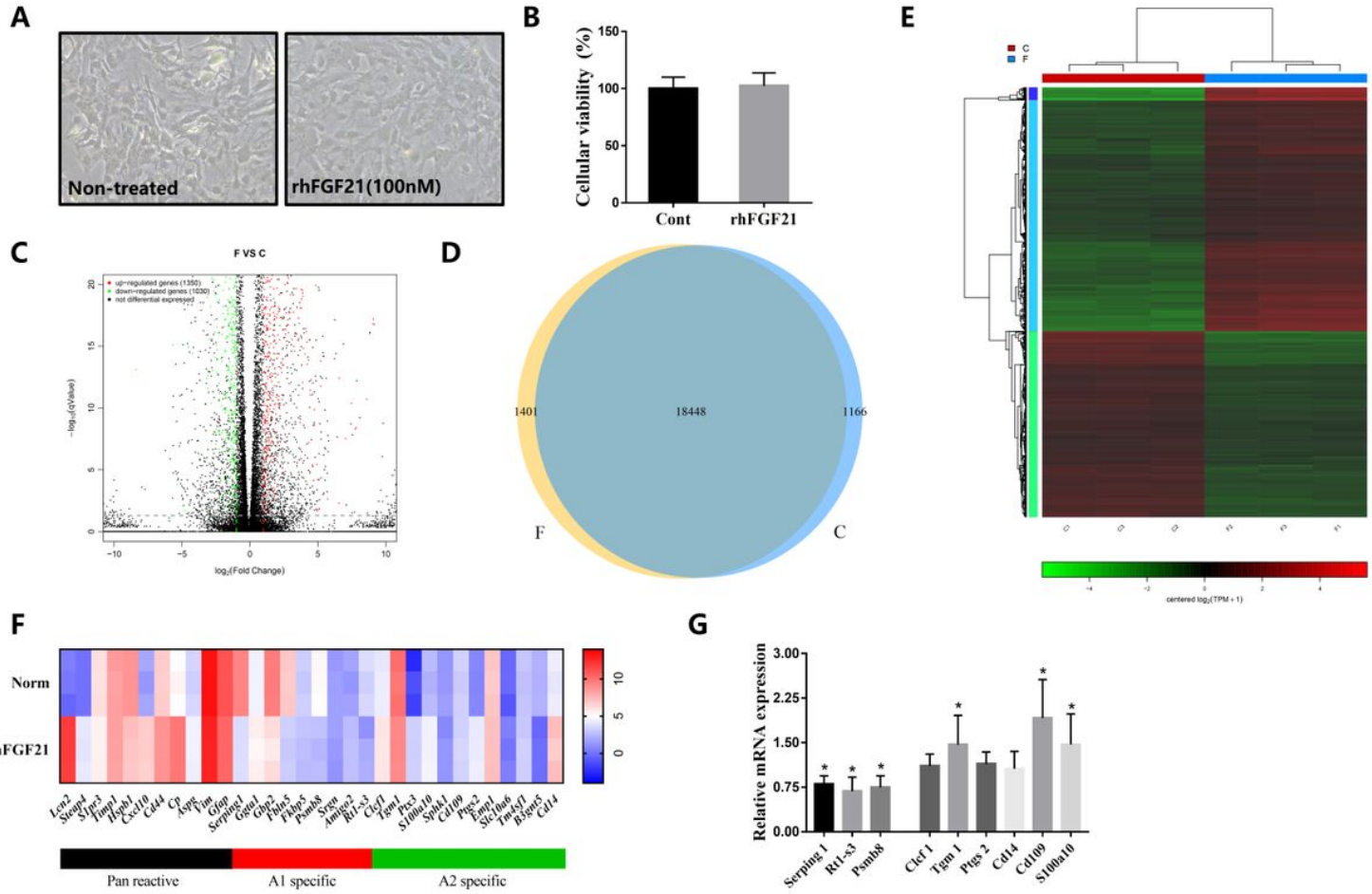

Figure 4

. rhFGF21 modulates the astrocytic phenotype. (A and B) Morphology and astrocytic viability after treatment with 100 nM rhFGF21. (C) Volcano plot of the differentially expressed genes. The red dots represent significantly upregulated genes, and the green dots represent downregulated genes. (D) Venn diagram of the differentially expressed genes between the Norm and rhFGF21 groups. The total number of genes in each group is represented by the sum of the two numbers in each circle, and the overlapping portions of the two circles indicate the expressed genes shared between the two groups. (E) Clustering heatmap of the differentially expressed genes between the two groups. (F) Heatmap of the reactive transcript levels of astrocytic phenotype genes. (G) A1 marker (Serping1, Rt1-s3, and Psmb8) and A2 marker (Clcf1, Tgm1, Ptgs2, Cd14, Cd109, and S100α10) mRNA levels. *P<0.05 vs the Cont group (one-way ANOVA); n=7.

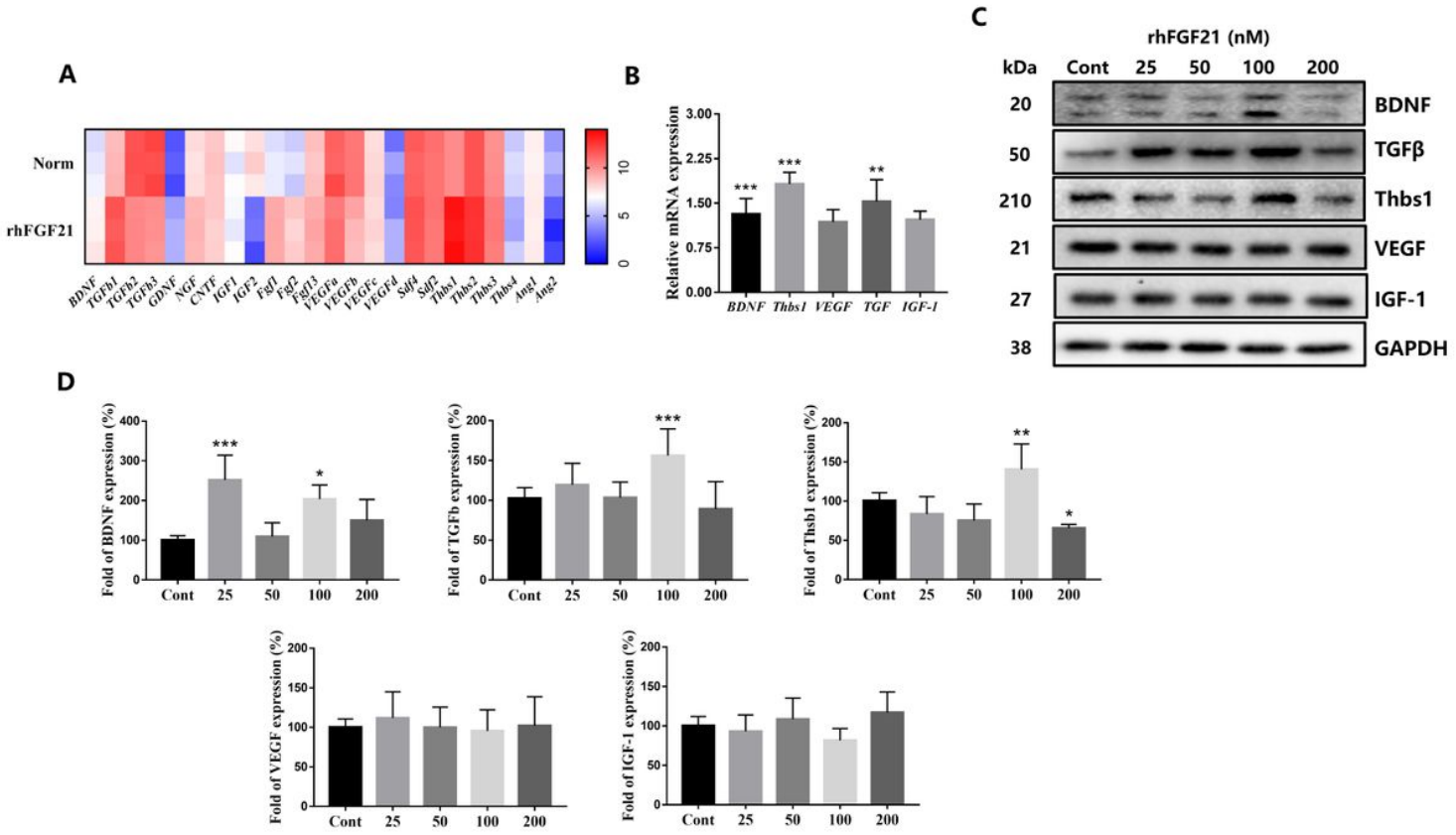

Figure 5

rhFGF21 increases trophic factor production in astrocytes. (A) Heatmap of astrocytic trophic factor reactive transcripts. (B) mRNA levels of BDNF, Thbs-1, VEGF, TGF-β, and IGF-1 after rhFGF21 treatment for 4 h. **P<0.01 and ***P<0.001 vs the Cont group (one-way ANOVA); n=6. (C and D) Representative Western blot images and quantification of BDNF, TGFβ, Thbs-1, VEGF, and IGF-1 in cell lysates after rhFGF21 treatment for 24 h. *P<0.05, **P<0.01, and ***P<0.001 vs the Cont group (one-way ANOVA); n=6.

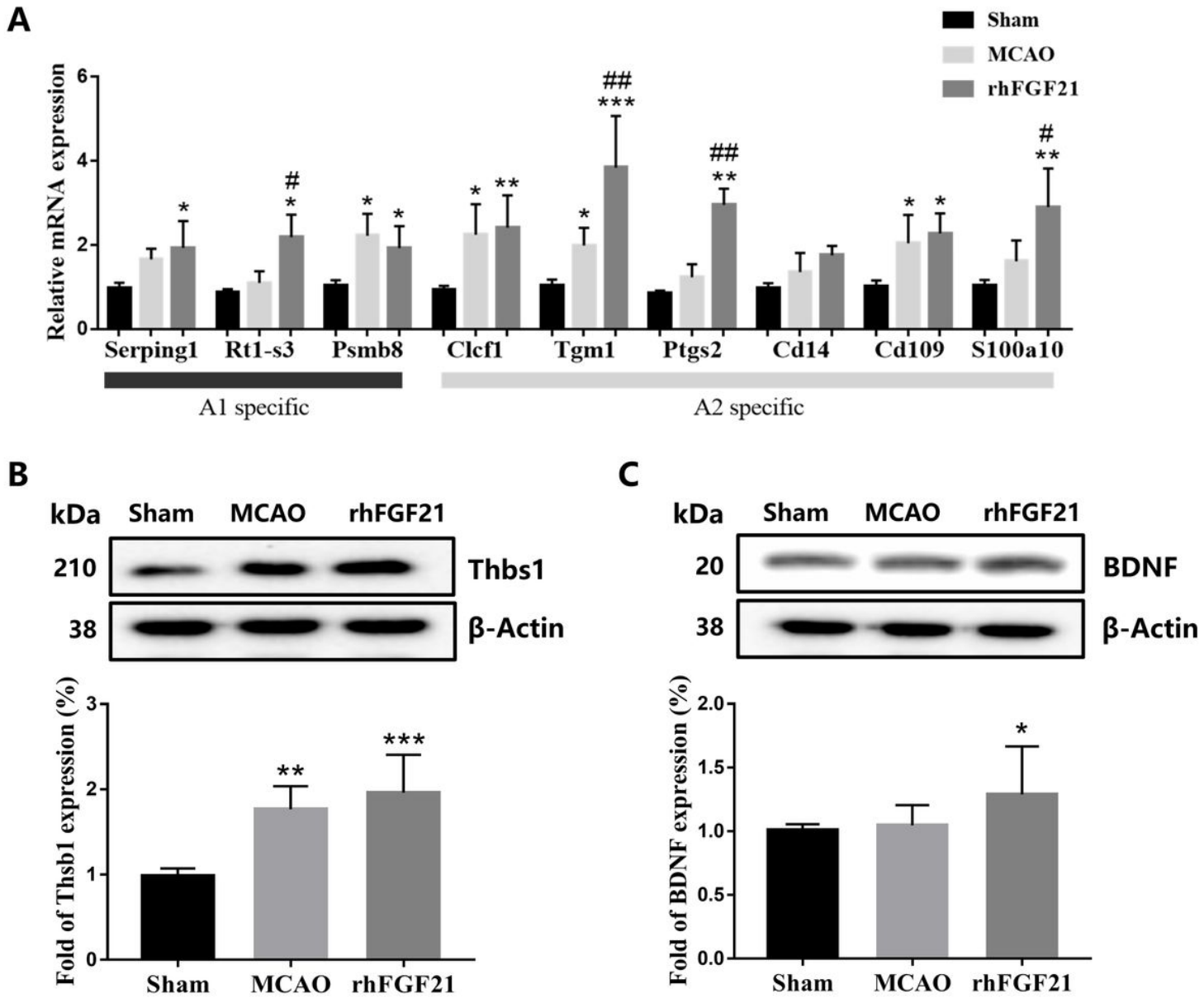

Figure 6

rhFGF21 modulates the astrocytic phenotype and increases trophic factor production in brain. (A) A1 marker (Serping1, Rt1-s3, and Psmb8) and A2 marker (Clcf1, Tgm1, Ptgs2, Cd14, Cd109, and S100α10) mRNA levels. *P<0.05, **P<0.01 vs the Sham group; #P<0.05, ##P<0.01 vs the MCAO group (one-way ANOVA); n=6. (B and C) Representative Western blot images and quantification of BDNF and Thbs1 in the cortical penumbra. *P<0.05, **P<0.05, ***P<0.01 vs the Sham group vs the MCAO group (one-way ANOVA); n=6.

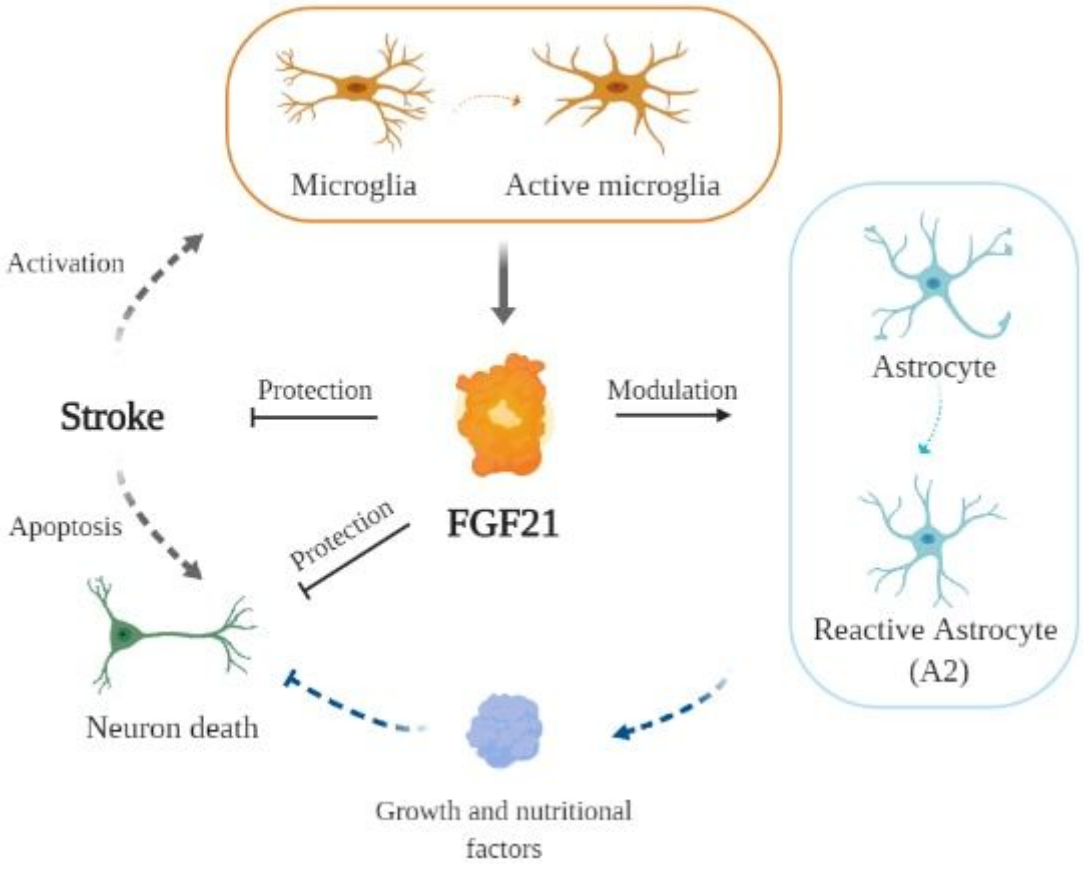

Figure 7

Proposed framework for the neuronal protective effects of FGF21 against ischemic injury. FGF21 from injured microglia ameliorates ischemic injury, and rhFGF21-activated astrocytes modulate pro-recovery phenotypes that are neuroprotective and promote neuroplasticity.